Electrodeposition of Polyphasic Films of Zinc Oxi Sulfide from DMSO onto n-InP(100) and n-InP(111) Single Crystals in the Presence of Zinc Salt, Thiourea, and Dissolved Molecular Oxygen

Rodrigo Henríquez,*,† Michele Froment,‡ Gonzalo Riveros,§ Enrique A. Dalchiele,|| Humberto Gómez,† Paula Grez,† and Daniel Lincot⊥

Instituto de Química, Facultad de Ciencias, Pontificia Universidad Católica de Valparaíso, Casilla 4059, Valparaíso, Chile, Laboratoire de Physique des Liquides et Electrochimie (UPR CNRS 7575), Université Pierre et Marie Curie, 4 Place Jussieu, 75232 Paris CEDEX 05, France, Facultad de Ciencias, Universidad de Valparaíso, Avda. Gran Bretaña 1111, Playa Ancha, Valparaíso, Chile, Instituto de Física, Facultad de Ingeniería, Herrera y Reissig 565, C.C. 30, 11000 Montevideo, Uruguay, and Laboratoire d'Electrochimie et Chimie Analytique (UMR CNRS 7575), Ecole Nationale Supérieure de Chimie de Paris, 11 Pierre et Marie Curie, 75321 Paris CEDEX 05, France

Received: December 11, 2006; In Final Form: January 26, 2007

In the present work, we studied the electrodeposition of zinc oxide sulfide films onto monocrystalline n-InP-($\bar{1}\bar{1}\bar{1}$) and (100) substrates starting from the combined reduction of thiourea, as a sulfide ion source, and molecular oxygen in the presence of zinc ions using DMSO as the solvent. The possible reactions involved in the formation of the films were studied through cyclic voltammetry. Independent of electrodeposition potential or the crystalline plane employed, a peculiar honeycomb bee morphology was observed by SEM in the deposits. The films formed on both crystalline planes showed a variable composition that can be adjusted by changing the electrodeposition potential. The crystalline characterization of the films was studied through RHEED. In agreement with the atomic ratio obtained by EDS, the patterns obtained showed that the as-grown deposits are basically formed by ZnO, ZnO_2, and ZnS. The polyphasic film composition can be represented by $[(ZnO)_a(ZnO2)_b(ZnS)_c]$, and a general formation reaction for this class of mixtures is proposed. The analysis of their optical properties for the polyphasic films formed onto FTO electrode gave a band gap of 3.46 eV, meaning that the films can be considered as a good alternative to a layer window in solar cells.

1. Introduction

Transparent thin films based on zinc oxide or zinc sulfide are of technological importance for solar cells, chemical sensors, liquid crystal displays, and as nanoporous films for dye sensitized solar cells.[1] Metal oxide thin films can be deposited by a wide variety of techniques including pulsed laser deposition, sputtering, e-beam evaporation, metal organic chemical vapor deposition (MOCVD), molecular beam epitaxy, spray pyrolysis, and solution methods.[1−3] The latter include sol−gel synthesis,[4] chemical solution deposition,[5] and electrodeposition.[6] Electrochemical synthesis of semiconductor films from aqueous and nonaqueous baths is of field growing interest,[7] where cathodic and anodic electrodeposition can be used to form oxide thin films. A common difficulty with anodic film growth is that the growing semiconductor film itself (as it presents a low conductivity) represents a barrier to further film growth that ultimately becomes self-limiting. Cathodic synthesis of metal oxides was introduced by Switzer to deposit ceramic thin films as well as powders.[8] Some aspects of the electrochemical synthesis of metal oxides and hydroxides have been reviewed recently.[9] Electrodeposited epitaxial films of ZnO,[10] Bi_2O_3,[11] Fe_3O_4,[12] and Cu_2O[13] grown onto gold single crystals have also been reported. ZnO is normally an n-type semiconductor with a room-temperature band gap about of 3.3 eV. Although stoichiometric ZnO films are highly resistive, highly conducting films can be made either by creating oxygen vacancies, which act as donors, or by doping with Al, Ga, or In.

ZnS is a wide band gap and direct transition semiconductor[14] that is a promising material for photoluminescent and electroluminescent devices,[15] detectors, emitters, and modulators.[16,17] It is used as window layer for thin-film heterojunction solar cells[18] and also is an important material for blue-light-emitting laser diodes.[19] Recently, ZnS thin films have been used as buffer layers in $CuInGaSe_2$-based solar cells and mini-models;[20] such films have been deposited by the chemical bath deposition (CBD) method, including some variations.[21−32] These films show band gap values between 3.0 and 4.0 eV. Moreover, the use of $Zn(O,S,OH)_x$ thin films as a buffer layer on Cu(InGa)-Se_2-based photovoltaic solar cells has been reported with very good results.[33] In fact, the photovoltaic community is expecting to achieve a 20% efficiency of $Cu(InGa)Se_2$-based devices using $Zn(O,S,OH)_x$ in place of CdS.[34]

A very small number of publications dealing with the electrodeposition of ZnS thin films from a nonaqueous-based electrolyte can be found in the literature. The use of a nonaqueous media exhibits several advantages and attributes: (i) the employment of a working temperature over 100 °C, (ii) a wider electrochemical potential window than that accessible in aqueous media, and (iii) it allows the electrochemical reduction of ionic and molecular precursors with formation of

* Corresponding author. E-mail: rodrigo.henriquez@ucv.cl.
† Pontificia Universidad Católica de Valparaíso.
‡ Université Pierre et Marie Curie.
§ Universidad de Valparaíso.
|| Instituto de Fisica.
⊥ Ecole Nationale Supérieure de Chimie de Paris.

10.1021/jp068511g CCC: $37.00
Published on Web 04/03/2007

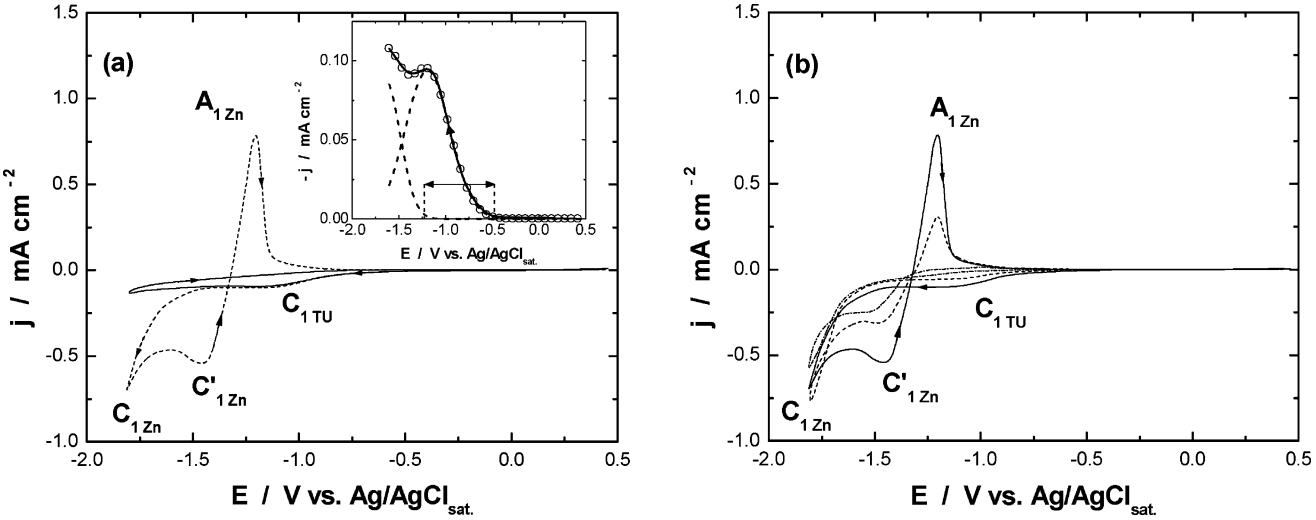

Figure 1. (a) Cyclic voltammogram of a FTO electrode on (—) TU 0.01 mol L^{-1} and (----) TU 0.01 mol L^{-1} + $ZnCl_2$ 5.0 × 10^{-3} mol L^{-1} at 373 K, v: 0.01 Vs^{-1}. Inset: deconvolution of cathodic hemicycles of the to DMSO system. (b) Continuous voltammetric cycled of the FTO electrode in the Zn^{2+}/TU/DMSO system under the same condition in Figure 1a: (—) first, (----) third, and (-·-·-) fifth cycles are shown.

the sulfide anion. These reactions cannot usually be carried out in aqueous media because of the electrochemical reduction of the solvent. A successful synthesis of ZnS depends then on the adsorption of S^{2-} onto the working electrode surface. This point has already been reported on InP substrates by Lincot et al.[35] Two examples can be shown for these precursors. Initially, Y. Tsukasa et al.[36] employed the electrochemical reduction of the thiocyante ion in aqueous media for the CdS synthesis. These authors showed that the reduction of sulfur is possible because of the catalytic effect of the metallic center in the complex ion. The electrochemical reaction that governs the process can be written as

$$[M(SCN)_4]^{2-} + 2e^- \rightarrow MS + CN^- + 3SCN^- \qquad (1)$$

Thiourea (TU) is another S^{2-} precursor potentially useful for achieving the electroformation of ZnS films. Notwithstanding, because of the high cathodic potential needed for this purpose, a reduced number of papers have been devoted to the electrochemical reduction of this molecular precursor. In fact, the formation of metallic sulfides from TU has only been observed at a mercury electrode in aqueous media.[37]

In this paper, we report on the electrodeposition and characterization of polyphasic films of $[(ZnO)_a(ZnO2)_b(ZnS)_c]$ formed on InP monocrystalline substrates in DMSO medium at 373 K. The films were prepared through the thiourea reduction as a source of sulfide ions and from the oxygen reduction dissolved to saturation at the working temperature. The possibility of an epitaxial growth of the ZnS phase onto InP was explored and evaluated by RHEED analysis.

2. Experimental Section

All chemicals used were analytical grade. The polyphasic films were obtained from a DMSO (PROLABO ≥ 99%) solution containing 5 × 10^{-3} mol L^{-1} $ZnCl_2$ (Aldrich 99.999%), 0.01 mol L^{-1} $SC(NH_2)_2$ (TU, Merck, ≥ 99%), and 0.100 mol L^{-1} LiCl (Aldrich 99.99%) as the supporting electrolyte. The temperature was held at 373 K by a thermostat to prevent the thermal decomposition of TU. The content of molecular oxygen was adjusted by bubbling with O_2 (Indura, 99,9%) for 30 min before each electrodeposition, and a positive atmosphere of oxygen was maintained during the electrochemical experiment. The concentration of dissolved molecular oxygen in DMSO was determined from the cathodic charge involved in the electrochemical wave of oxygen reduction onto a glassy carbon electrode under potentiodynamic conditions; the estimated value was around 0.75 × 10^{-3} mol L^{-1}. Glass covered with a thin film of tin oxide doped with F, n-type $(\bar{1}\bar{1}\bar{1})$ InP (phosphorus face), and (100) InP single crystals of 0.08 Ωcm were used as substrates. InP substrates were purchased from the Institute of Electronic Materials Technology. They were n-type doped at a level of 10^{16} cm^{-3}. The following surface treatments were used prior to electrodeposition:

- The SnO_2/F glasses were washed successively with acetone, a 50% v/v HNO_3/water solution, and then rinsed thoroughly with deionized water (Millipore).
- The InP substrates were cleaned first during 10 min in boiling acetone, then 3 min in boiling methanol, and 3 min in methanol at room temperature. Afterward, without drying the surface, they were etched for 20 s in a 0.40% bromine in methanol solution. Finally, they were rinsed with methanol and deionized water. Before the deposition, the surface oxide was removed during 5 min in 3.0 M sulfuric acid solution.[38,39]

All of the substrates were dried with argon before introducing them into the electrochemical cell. Electrochemical studies as well as film deposition experiments were made using a conventional three-electrode electrochemical cell connected to an AUTOLAB PGTAT20 potentiostat. A platinum wire separated by a glass frit was used as the counter electrode, and a $Ag/AgCl_{sat}$ electrode was used as a reference ($E°_{Ag/AgCl}$ = + 0.194 vs NHE).

Optical transmission measurements on SnO_2/F (FTO) covered glass substrates were carried out using a SHIMAZDU UV-160 A double-beam spectrophotometer. Spectra were recorded at room temperature against air as a reference.

Scanning electron microscopy (SEM) and energy dispersive X-ray analysis (EDS) were carried out using a NORAN Z-Max 30 instrument. Reflection of high-energy electron diffraction (RHEED) studies were conducted with a Jeol JEM-100Cx II model working at 100 kV.

3. Results and Discussion

3.1. Voltammetric Analysis. To understand the electrochemical responses of the system, the electrochemical behavior of TU in the absence of oxygen was studied. Figure 1 shows the voltammetric response of a FTO electrode in the TU/DMSO

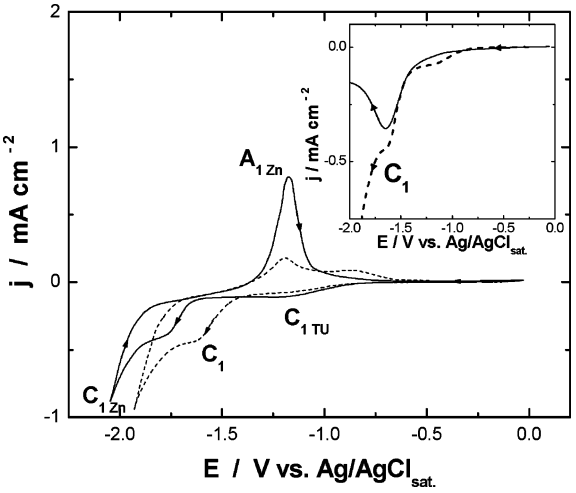

Figure 2. Comparison of the potentiodynamic response for the Zn^{2+}/TU/O_2 system: TU 0.01 mol L^{-1}, $ZnCl_2$ 5.0×10^{-3} mol L^{-1} in DMSO at 373 K, v: 0.01 V s^{-1} on the (----) n-InP(100) and (—) n-InP($\bar{1}\bar{1}\bar{1}$). Inset: comparison of the cathodic potentiodynamic response in the systems (—) O_2/DMSO and (---) Zn^{2+}/TU/O_2/DMSO onto n-InP(100) at 373 K, v: 0.01 V s^{-1}.

system in the presence and absence of zinc ions. In the first case, the cathodic current onset is at −0.50 V, which further develops in a well-defined peak at −1.19 V (marked as $C_{1\ TU}$ in Figure 1a). This peak can be associated to TU electrochemical reduction according to[37]

$$TU + 2e^- \rightarrow S^{2-} + CN^- + NH_4^+ \quad (2)$$

which is probably under diffusion control. The absence of anodic peaks in the reverse scan indicates the irreversibility of the TU/S^{2-} couple. The lack of other signals with the continuous cycling (i.e., S^{2-}/S_2^{2-} couple) indicates that the sulfide ion is not adsorbed at the electrode surface. In fact, S^{2-} diffuses to the solution bulk due to the low perturbation sweep rate. Alternatively, anodic signals associated to the electrochemical oxidation of TU to its formamidine disulfide dimmer (FDS) were not observed under the conditions of the experiment.

The electrochemical reduction of TU is not affected by the presence of zinc ions. The reduction of the latter takes place at −1.43 V (marked as $C_{1\ Zn}$ in Figure 1a), thus giving a wide potential window (see the inset of Figure 1a) for the deposition of ZnS via a precipitation reaction under supersaturation conditions. Zn^{2+} reduction is produced again in the reverse scan ($C'_{1\ Zn}$) but now onto the previously metallic zinc islands electrodeposited at the electrode surface during the cathodic sweep. The presence of this $C'_{1\ Zn}$ process could be related to the formation of an insulating ZnS layer. The anodic peak ($A_{1\ Zn}$) appearing at −1.25 V can be assigned to the striping of the metallic zinc previously formed at the substrate. Furthermore, no other electrochemical features during the rest of the anodic scan are observed. Confirming the assumption that an insulating layer was formed within this potential window, the ratio of the anodic to cathodic charges associated to the zinc electrochemical processes, calculated as $(Q_{C_{1\ Zn}} + Q_{C'_{1\ Zn}})/Q_{A_{1\ Zn}}$, is equal to 1.03. Furthermore, the charge diminution observed for each one of the processes involved when the FTO electrode undergoes repetitive potential scans (Figure 1b) is coherent with the formation of a large band gap semiconductor as is the case for ZnS (i.e., 3.66 eV).

The voltammetric response of the Zn^{2+}/TU/O_2/DMSO system onto a monocrystalline n-InP was studied further. Figure 2 shows the potentiodynamic profiles of n-InP electrodes for the ($\bar{1}\bar{1}\bar{1}$) and (100) preferentially oriented crystalline planes. In general, three reduction processes can be observed: the electrochemical processes $C_{1\ TU}$ and $C_{1\ Zn}$ previously found on the FTO electrode, and a new cathodic wave, marked as C_1. This new cathodic process can be explained by comparing the cathodic hemicycle responses recorded onto the (100) plane for systems O_2/DMSO and Zn^{2+}/TU/O_2/DMSO, respectively (see the inset of Figure 2). When only oxygen is present, an electrochemical reduction process is observed in the same potential interval of the pick marked as C_1. This wave can be attributed to the electrochemical reduction of oxygen according to the following electrochemical−chemical mechanism:[40,41]

$$O_2 + e^- \rightarrow O_2^- \quad (3)$$

$$2O_2^- \rightarrow O_2 + O_2^{2-} \quad (4)$$

In the presence of Zn^{2+}, both reactions can contribute to the formation of ZnO_2 at the electrode surface, and then the possible formation of a new insulating film should be considered. Moreover, as has been demonstrated by G. Hodes et al.,[7] the ZnO formation cannot be discarded. Then, according to the conditions in which the experiment is carried out, the possible formation of a ZnS−ZnO−ZnO_2 mixture onto the monocrystalline substrate should also be considered.

The potential at which the processes $C_{1\ Zn}$ and C_1 take place changes according to the InP crystalline plane involved in the film electrodeposition. They appear at a more cathodic potential at the ($\bar{1}\bar{1}\bar{1}$) n-InP than at the (100) n-InP planes (i.e., 0.20 V). Alternatively, the potential of peak $C_{1\ TU}$ appears at the same potential position on both electrodes, but the current density is slightly higher on ($\bar{1}\bar{1}\bar{1}$) n-InP (see Figure 2). According to the previous discussion, the potential shifting can be related to the formation of a more insulating layer onto the ($\bar{1}\bar{1}\bar{1}$) planes; a greater overpotential is then required in order to develop these processes. This assumption is feasible because the $C_{1\ TU}$ process is not affected by the crystallographic orientation. Moreover, it is also supported by the fact that the greater current density observed in the ($\bar{1}\bar{1}1$) plane would produce an increase in the kinetics of S^{2-} formation due to the electrochemical reduction of TU. This would lead to the growth of a more insulating film at this substrate.

In the reverse scan, the stripping of Zn (peak $A_{1\ Zn}$) appears as a single well-defined peak onto the ($\bar{1}\bar{1}1$) n-InP surface and as a double peak onto the (100) n-InP plane. In spite of this different voltammetric response, in both cases the same cathodic to anodic charge ratios for the zinc processes are found in both cases. For (100) n-InP, this is an indication that the splitting of the $A_{1\ Zn}$ peak is still correlated with this metallic precursor and not with the stripping of superficial metallic indium formed by the decomposition of the semiconductor substrate.[39]

3.2. Electrodeposition of Thin Films on n-InP Substrate. According to the voltammetric study, the potential windows at which thin films can be electrodeposited are −1.40 to −1.80 V for the ($\bar{1}\bar{1}\bar{1}$) n-InP and −1.20 to −1.60 V for (100) n-InP. Figure 3 shows the current/time transients obtained during the potentiostatic electrodeposition of the films at both monocrystalline substrates. The current fluctuation observed in the curves is due to a strong change in the electroactive electrode area during the formation of the film. Moreover, because of the low O_2 concentration in the bath (i.e., 0.75×10^{-3} mol L^{-1}) these j/t transients show that at the lowest deposition potentials (i.e., −1.40 and −1.20 V for ($\bar{1}\bar{1}\bar{1}$) and (100) crystalline planes, respectively) the process is controlled by the molecular oxygen

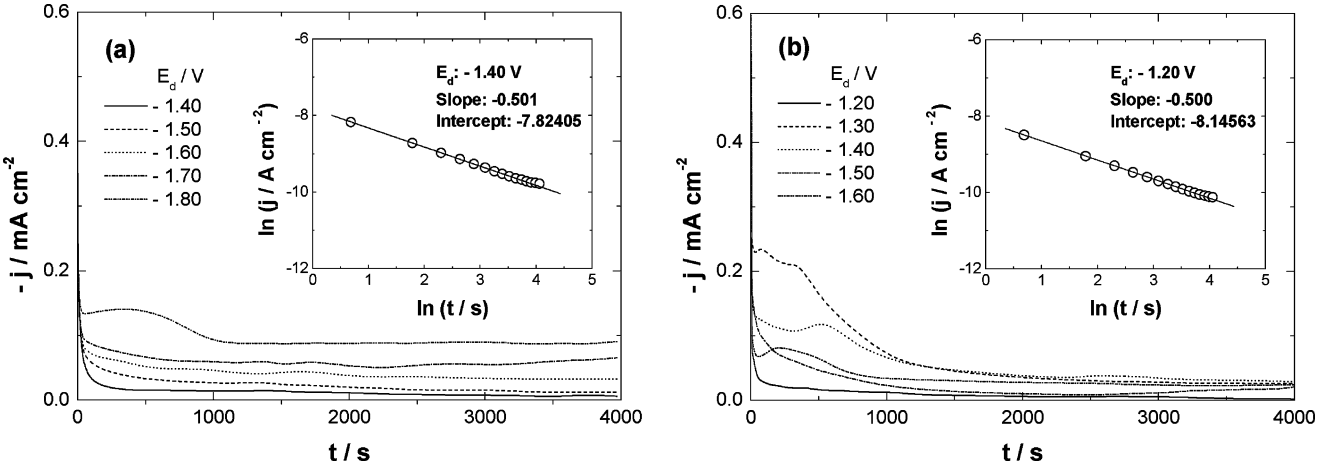

Figure 3. j/t transient obtained in the film electrodeposition in the $Zn^{2+}/TU/O_2$ system in DMSO on (a) n-InP($\bar{1}\bar{1}\bar{1}$) and (b) n-InP(100). TU: 0.01 mol L^{-1}, Zn^{2+}: 5.0×10^{-3} mol L^{-1} in DMSO at 373 K. The deposition potentials are indicated in the same figures; the insets show the linear representation of the Cottrell equation and the simulation parameters obtained during the first 60 s of polarization.

TABLE 1: Diffusion Coefficient Values for O_2 in DMSO Calculated from the Cottrell Equation by Simulation of the *j/t* Transient Obtained to a More Anodic Electrodeposition Potential[a]

$-E_d$/V	n-InP plane	$(n_{O_2}FD^{1/2}C^{\infty}_{O_2})/(\pi^{1/2})$ (A $s^{1/2}$ cm^{-2})	D_{O_2} (cm^2 s^{-1})
1.20	(100)	0.00029	5.04×10^{-5}
1.40	($\bar{1}\bar{1}\bar{1}$)	0.00040	9.60×10^{-5}

[a] For the simulation as considered: $n_{O_2} = 1$, $C^{\infty}_{O_2} = 0.75 \times 10^{-6}$ mol cm^{-3}, and $F = 96\,500$ C mol^{-1}.

diffusion toward the electrode surface. This was verified by simulation of the j/t curves at two electrodeposition potentials (E_d) in the first 60 s employing the Cottrell equation (5).

$$j\left[\frac{A}{cm^2}\right] = \left(\frac{n_{O_2}FD^{1/2}_{O_2}C^{\infty}_{O_2}}{\pi^{1/2}}\right)\left[\frac{As^{1/2}}{cm^2}\right] t^{-1/2}[s^{-1/2}] \qquad (5)$$

The diffusion coefficients for molecular oxygen (D_{O_2}) and the simulation parameters obtained from the fitting procedure are summarized in Table 1. These values are comparable with the diffusion coefficient reported for molecular oxygen in water (i.e., $D_{O_2} = 2 \times 10^{-5}$ cm^2 s^{-1}).[42] This demonstrates that oxygen mobility is comparable in both solvents probably because of favorable intermolecular interactions. Alternatively, the small differences observed in the D_{O_2} value can only be associated either to the error of the determination or to a decrease in the oxygen concentration due to a possible chemical oxidation of TU. However, in agreement with the potentiodynamic experiences carried out in the system, it was not possible to observe the presence of formamidine disulfide dimmer (FDS) to confirm this hypothesis. Finally, the inset in Figure 3 shows that when $t > 60$ s notorious deviations take place in the linear response of the Cottrell equation. This confirms the formation of an insulating film whose growth may depend on the preferential orientation of the substrate. In fact, when the cathodic currents are compared in this time interval (i.e., first 60 s), the ($\bar{1}\bar{1}\bar{1}$) n-InP plane emerges as more active with respect to the (100) n-InP one.

3.3. Morphological and Composition Characterization of the Thin Films. When E_d was more anodic than -1.55 V for (100) n-InP and -1.70 V for ($\bar{1}\bar{1}\bar{1}$) n-InP crystalline planes, the presence of a transparent film was observed at the substrate surfaces. The absence of color is coherent with the optical properties of films with wide band gap energies that absorb in the UV region. In fact, the study of the optical properties of the films grown onto FTO electrodes in the same conditions (through the relationship $(\alpha l \cdot h\nu)^2$ vs $h\nu$) gives a band gap of 3.46 eV. Considering the values of band gaps energies reported (3.37 eV for ZnO,[43] 3.69 eV for ZnO_2,[44] and 3.66 eV for ZnS [45]) it is clear that the value obtained for the films can correspond to some of the mentioned phases. Alternatively, possibly because of the presence of metallic zinc excess, films grown at more cathodic potential present a gray color.

Figure 4 shows the SEM micrographs of thin films electrodeposited at -1.50V at ($\bar{1}\bar{1}\bar{1}$) and (100) crystallographic orientations of n-InP substrates. The layer formed at the former (see Figure 4a) shows an irregular morphology characterized by cell structures extended along the whole deposit surface as a honeycomb of bees. The cells have a regular size of approximately 20×20 nm^2. This situation is not altered by the electrodeposition potential employed in film electrosynthesis. A similar situation is found for the deposits obtained onto the (100) n-InP plane (see Figure 4b), but the deposits present aggregations distributed on the surface. Alternatively, the existence of a significant quantity of dark zones can be seen on the surface. In agreement with previous voltammetric analysis and RHEED studies (vide infra), these zones can be an indication of metallic zinc formation.

Table 2 shows the EDS composition of the electrodeposited thin films onto n-InP($\bar{1}\bar{1}\bar{1}$) as a function of E_d. Irrespective of the E_d value, an unexpected oxygen atomic composition of ca. 50% can be observed. Moreover, although the zinc atomic concentration was between 38 and 48%, there is a very low sulfur atomic concentration in the same potential range; the only possibility through which the sulfur must be found is under the form of a ZnS phase. The relation between the oxygen atomic concentration and the remaining zinc (not forming ZnS) is also shown in Table 2. As will be discussed further in the RHEED discussion section, because E_d is made more negative this ratio increased from 1.16 to 1.85, probably because of the formation of a ZnO and/or a ZnO_2 phase.

Table 3 shows the EDS composition of the electrodeposited thin films onto n-InP(100) as a function of the growth potential, revealing a behavior similar to that observed in the case of n-InP($\bar{1}\bar{1}\bar{1}$) but the oxygen atomic concentration is lower than 50%. As was discussed above, the electrochemical reduction of zinc ions onto the (100) plane shifts in the anodic direction; then, at the same electrodeposition potential values, films richer in zinc and poorer in oxygen can be obtained. Under these

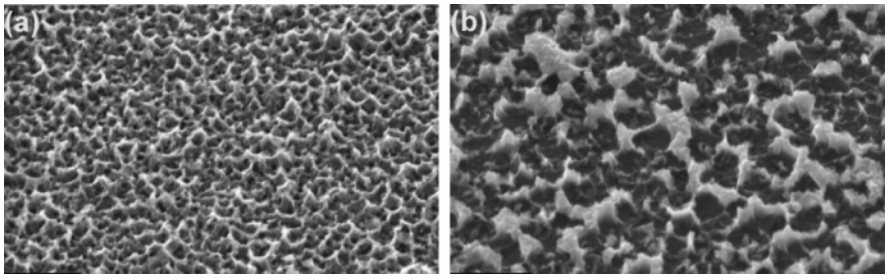

Figure 4. SEM images obtained to −1.50 V: (a) 6.16 × 3.84 μm^2 on n-InP($\bar{1}\bar{1}\bar{1}$) and (b) 7.11 × 4.43 μm^2 on n-InP(100). In both cases, the amplification used was 15000× and the deposition charge passed was 0.50 C cm^{-2}.

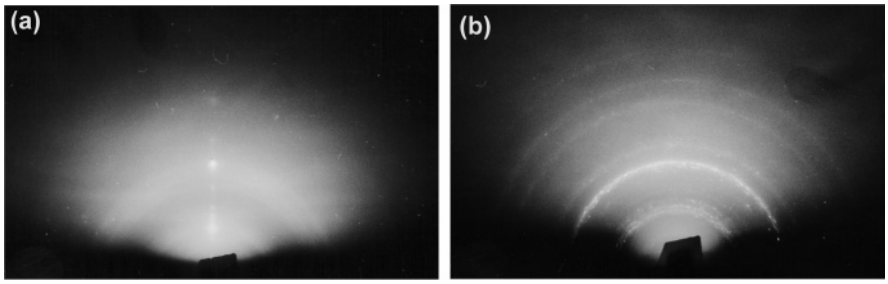

Figure 5. RHEED patterns for two deposits on n-InP($\bar{1}\bar{1}\bar{1}$) observed along the azimuth <1$\bar{1}$0>; (a) −1.65 V and (b) −1.80 V. The deposition charge in both cases was 0.50 C cm^{-2}.

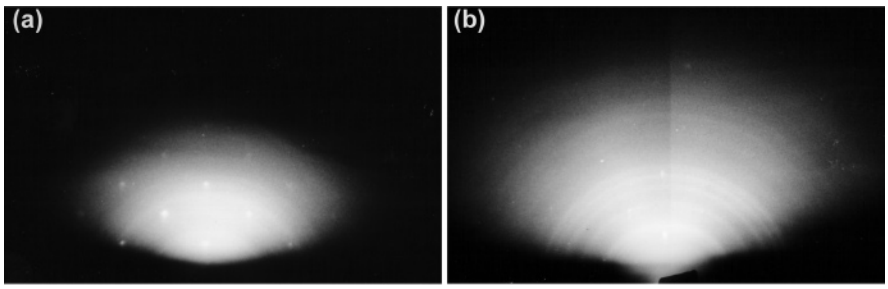

Figure 6. RHEED patterns for two deposits on n-InP(100) observed along the azimuth <0$\bar{1}$1>; (a) −1.20 V and (b) −1.40 V. The deposition charge in both cases was 0.50 C cm^{-2}.

TABLE 2: Atomic Composition Obtained by EDS Analysis for the Deposit Formed on n-InP($\bar{1}\bar{1}\bar{1}$)[a]

$-E_d$/V	%At Zn	%At S	%At O	$(\%At_O)/(\%At_{Zn} - \%At_S)$	estimated thickness by EDS (nm)
1.50	46.9	8.3	44.8	1.16	89
1.55	43.5	6.8	49.7	1.35	102
1.60	43.9	6.9	49.2	1.33	132
1.65	43.3	10.1	46.6	1.40	124
1.70	42.1	10.1	47.8	1.49	150
1.80	38.1	10.2	51.7	1.85	153

[a] In all cases, the deposition charge used was 0.50 C cm^{-2}.

TABLE 3: Atomic Composition Obtained by EDS Analysis for the Deposit Formed on n-InP(100)[a]

$-E_d$/V	%At Zn	%At S	%At O	$(\%At_O)/(\%At_{Zn} - \%At_S)$	estimated thickness by EDS (nm)
1.20	38.9	10.4	50.8	1.78	104
1.30	43.4	11.7	44.9	1.42	92
1.40	52.7	22.6	24.7	0.82	118
1.50	56.6	15.8	27.6	0.67	137
1.60	57.4	16.7	25.9	0.64	125

[a] In all cases, the deposition charge used was 0.50 C cm^{-2}.

circumstances, the presence of a ZnS + ZnO + ZnO_2 mixture phase is feasible. Moreover, at more cathodic potential values the presence of metallic zinc can also be predicted. The low sulfur atomic concentration observed in the electrodeposited films on both monocrystalline substrates can probably be due to two factors: (i) the slow reduction kinetics of TU on both substrates as compared with the reduction oxygen process under potentiostatic condition and (ii) the natural diffusion of sulfide ion toward the bulk of the solution. This prevents an oversaturation condition for favoring the heterogeneous precipitation of the ZnS phase at both InP crystalline planes.

3.4. RHEED Analysis. RHEED analyses were carried out to characterize the phase composition and the structural and crystalline quality of the films. Figure 5 shows the RHEED patterns of thin films electrodeposited onto n-InP($\bar{1}\bar{1}\bar{1}$) substrates at −1.65 and −1.80 V. A study of the different phases present in the films and a quantitative analysis of these patterns were accomplished, and the results are depicted in Table 4. The presence of a mixture of the following phases was found: hexagonal ZnO, cubic ZnO_2, cubic ZnS, and tetragonal $Zn(OH)_2$, (i.e., $Zn_x(O,S,OH)_y$). The presence of the $Zn(OH)_2$ phase can be attributed either to the film contamination with products coming from the reduction of water present in DMSO media or to an instability of the ZnO_2 phase in the humid environment. This compound is present only in films that have been deposited at more anodic potentials; but in the basis of the EDS analysis, the formation of this phase at more cathodic potentials cannot be precluded, perhaps present as an amorphous phase not detected by the RHEED. As a general rule, independent of the electrodeposition potential, the diffraction patterns are consti-

TABLE 4: Diameter of Semicircles Obtained in the RHEED Patterns for the Polyphasic Films Deposited on n-InP($\bar{1}\bar{1}\bar{1}$)[a]

$-E_d$/V	line	intensity (au)	diameter (mm)	experimental d(h,k.l) (Å)	theoretical d(h,k.l) (Å)	(h,k,l) assignment
1.65	L1	S	34	3.25	3.25	(109) − $Zn(OH)_2$ tetragonal ?
	L2	M	40	2.76	2.80	(111) − ZnO_2
	L3	M	45	2.46	2.46	(101) − ZnO hexagonal
	L4	W	57	1.94	1.91/1.98	(102) − ZnO hexagonal/ (211)− ZnO_2
	L5	S	76	1.45	1.47	(311) − ZnO_2
	L6	W	115	0.96	0.96	(440) − β-ZnS cubic
1.80	L7	W	39	2.84	2.80	(111) − ZnO_2
	L8	W	45	2.46	2.48	(101) − ZnO hexagonal
	L9	S	68	1.63	1.63	(311) − β-ZnS cubic
	L10	M	81	1.36	1.35	(400) − β-ZnS cubic
	L11	W	108	1.02	1.04	(511) − β-ZnS cubic
	L12	W	116	0.95	0.96	(440) − β-ZnS cubic

[a] The K value employed for the d(h,k,l) determination was 110,58 Å mm. W, weak; M, medium; and S, strong.

TABLE 5: Diameter of Semicircles Obtained in the RHEED Patterns for the Polyphasic Films Deposited on n-InP(100)[a]

$-E_d$/V	line	intensity (au)	diameter (mm)	experimental d(h,k,l) (Å)	theoretical d(h,k,l) (Å)	(h,k,l) assignment
1.20	L1	W	19	5.82	5.79	(103) − $Zn(OH)_2$ tetragonal ?
	L2	M	45	2.46	2.48	(101) − ZnO hexagonal
	L3	M	54	2.05	2.05/1.98	(307) − $Zn(OH)_2$ tetragonal ?/ (211) − ZnO_2
	L4	W	76	1.45	1.47	(311) − ZnO_2
	L5	W	82	1.35	1.35	(400) − β-ZnS cubic
1.40	L6	W	35	3.16	3.15	(304) − $Zn(OH)_2$ tetragonal ?
	L7	M	45	2.46	2.48	(101) − ZnO hexagonal
	L8	M	54	2.05	2.05/1.98	(307) − $Zn(OH)_2$ tetragonal ?/ (211)− ZnO_2
	L9	M	66	1.68	1.69	(10,2) − Zn hexagonal
	L10	M	76	1.45	1.47	(311) − ZnO_2
	L11	M	82	1.35	1.35	(400) − β-ZnS cubic
	L12	W	114	0.97	0.96/0.96	(400) − β-ZnS cubic/ (204) − ZnO hexagonal

[a] The K value employed for the d(h,k,l) determination was 110.58 Å mm. W, weak; M, medium; S, strong.

tuted of rings, indicating the polycrystalline character of the films. Moreover, the presence of several rings is an indication of the presence of several components forming the electrodeposited film. However, the diffraction pattern of Figure 5a shows in addition the presence of dots in the ($\bar{1}\bar{1}\bar{1}$) direction, indicating a texture growth in this crystallographic direction. Considering the thickness of the films reported in Tables 2 and 3, it is clear that the diffraction patterns are originated only from the films and not from the substrate. Taking into account the cubic, hexagonal, cubic, and tetragonal structures of ZnS, ZnO, ZnO_2, and $Zn(OH)_2$, respectively, and considering their respective lattice constants and those of the InP substrate, the lattice mismatch ($a_{film} - a_{Inp}/a_{Inp}$) between films and substrate can be determined. The calculated lattice mismatch values for ZnS/InP, ZnO/InP, ZnO_2/InP, and $Zn(OH)_2$/InP are 8%, −45%, −17%, and 40%, respectively. From these results explaining the dot patterns observed in Figure 5a, the epitaxy formation of a ZnS/InP heterostructure appears as more probable. In fact, this type of epitaxy is possible in conditions where the electrochemical reduction kinetics of TU is slow, that is, at the more anodic electrodeposition potentials. However, because of the oxygen reduction at the more cathodic potentials, the epitaxtial growth is not feasible and the RHEED pattern only shows rings, indicating the polycrystalline character of the film (see Figure 5b).

Figure 6 shows the RHEED patterns of the thin films electrodeposited onto n-InP(100) at −1.20 and −1.40 V. A quantitative analysis of the patterns was done, and the results are depicted in Table 5. In the present case, the presence of polycrystalline cubic ZnS, hexagonal ZnO, and cubic ZnO_2 can be observed. As compared with films deposited onto n-InP($\bar{1}\bar{1}\bar{1}$), the $Zn(OH)_2$ phase is present in the whole electrodeposition potential interval studied. Several rings and dots are present at the more anodic electrodeposition potential. As in the case of the electrodeposited layers onto n-InP($\bar{1}\bar{1}\bar{1}$), the epitaxial formation of ZnS thin films onto n-InP(100) is also evidenced. The epitaxial character disappears when the electrodeposition potential is made more cathodic (see Figure 6b). Moreover, at this more cathodic potential the presence of metallic zinc can be confirmed.

On the basis of the EDS and RHEED results, the following reaction can be proposed for the formation of the different phases present in the electrodeposited polyphasic thin films:

$$6Zn^{2+} + 2(NH_2)_2CS + 3O_2 + 6e^- \rightarrow 2[(ZnO)_a(ZnO2)_b(ZnS)_c] + 2CN^- + 2NH_4^+ \quad (6)$$

This general reaction takes place when the three components are present at the interface. In this way, the reduction of TU together with the oxygen reduction explains the composition of the resulting films.

4. Conclusions

Electrodeposition at controlled potential was employed to prepare polyphasic thin films starting from the combined

reduction of thiourea and oxygen in the presence of zinc ions in organic DMSO media. The analysis of RHEED patterns and the composition obtained by EDS showed that the films presented a strong tendency to form polycrystalline phases constituted by ZnO, ZnO_2, and ZnS. It is proposed that the presence of $Zn(OH)_2$ in the films can be related to the instability of the ZnO_2 phase with the environmental humidity. Independent of the InP monocrystalline plane employed as a substrate, the same RHEED patterns showed that the ZnS phase presents an epitaxial growth, in agreement with the low mismatch between both phases. However, epitaxy is lost when the deposition potential becomes more cathodic. The film composition can be varied through the deposition potential, but the honeycomb of bees morphology and the band gap remains unchanged. Considering the thickness of the films and the obtained E_g value (3.46 eV), the possibility exists of using this type of film as window layers in thin-film solar cells based on copper indium gallium diselenide absorbers.

Acknowledgment. We acknowledge FONDECYT - CHILE support (project no. 1060442). Special acknowledgements to the ECOS - CONICYT PROGRAM (project no. C00E02) between France and Chile governments.

References and Notes

(1) Jayakrishnan, R.; Hodes, G. *Thin Solid Films* **2003**, *440*, 19−25.
(2) Elidrissi, B.; Addou, M.; Regragui, M.; Bougrine, A.; Kachouane, A.; Bernède, J. C. *Mater. Chem. Phys.* **2001**, *68*, 175−178.
(3) Mokili, B.; Charreire, Y.; Cortes, R.; Lincot, D. *Thin Solid Films* **1996**, *288*, 21−28.
(4) Tang, W.; Cameron, D. C. *Thin Solid Films* **1994**, *238*, 83−87.
(5) Niesen, T. P.; De Guire, M. R. *J. Electroceram.* **2001**, *6*, 169−207.
(6) Katayama J.; Izaki M. *J. Appl. Electrochem.* **2000**, *30*, 855.
(7) Gal, D.; Hodes, G.; Lincot, D.; Schock, H. W. *Thin Solid Films* **2000**, *361*, 79−83.
(8) Switzer, J. A. *Bull. Am. Ceram. Soc.* **1987**, *66*, 1521−1524.
(9) Therese, G. H. A.; Kamath, P. V. *Chem. Mater.* **2000**, *12*, 1195−1204.
(10) Pauporte, Th.; Lincot, D. *Appl. Phys. Lett.* **1999**, *75*, 3817−3819.
(11) Switzer, J. A. *Science* **1999**, *284*, 293−296.
(12) Nikiforov, M. P.; Vertegel, A.; Shumsky, M. G.; Switzer, J. A. *Adv. Mater.* **2000**, *12*, 1351−1353.
(13) Bohannan, E. W.; Shumsky, M. G.; Switzer, J. A. *Chem. Mater.* **1999**, *11*, 2289−2291.
(14) Hass, G.; Heaney, J. B.; Hunter, W. R. In *Physics of Thin Films*; Francombe, M. H., Vossen, J. L. Eds.; Academic Press: New York, 1982; Vol. 12, pp 48−50.
(15) Mane, R. S.; Lokhande, C. D. *Mater. Chem. Phys.* **2000**, *65*, 1−31.
(16) Nicolau, Y. F.; Dupuy, M.; Brunel, M. *J. Electrochem. Soc.* **1990**, *137*, 2915−2924.
(17) Marquardt, E.; Optiz, B.; Scholl, M.; Henker, M. *J. Appl. Phys.* **1994**, *75*, 8022−8026.
(18) Dona, J. M.; Herrero, J. *J. Electrochem. Soc.* **1994**, *141*, 205−210.
(19) Hasse, M. A.; Qiu, J.; DePuydt, J. M.; Cheng, H. *Inst. Phys. Conf. Ser.* **1991**, *120*, 9−16.
(20) Sushiya, K.; Sugiyama, I.; Tachiyakai, M.; Kuse, T.; Nagoya, Y.; Okumura, D.; Sato, M.; Yamase, O.; Takeshita, H. *Proceedings of the Technical Diag. of the International PVSEC − 9*, Miyazaki, Japan, 1996, C-II-7.
(21) Biswas, S.; Pramanik, P.; Basu, P. K. *J. Mater. Sci. Lett.* **1986**, *5*, 1216−1218.
(22) Nair, P. K.; Nair, M. T. S. *Semicond. Sci. Technol*. **1992**, *7*, 239−244.
(23) The Chemical Society In *Stability Constant of Metal Ion Complexes, Suppl. 1*; Sillen, L. G., Martell, A. F. Eds.; Special Publication No. 25; Chemical Society: London, 1971.
(24) Ndukwe, I. C. *Sol. Energy Mater. Sol. Cells* **1996**, *40*, 123−131.
(25) Mokili, B.; Charreire, Y.; Cortes, R.; Lincot, D. *Thin Solid Films* **1996**, *288*, 21−28.
(26) Kitaev, G. A.; Uritskaya, A. A.; Belova, N. S. *Russ. J. Phys. Chem.* **2000**, *73*, 1507−1510.
(27) Froment, M.; Lincot, D. *Electrochim. Acta* **1995**, *40*, 1293−1303.
(28) Valkonen, M. P.; Kanniainen, T.; Lindroos, S.; Leskelä, M.; Rauhala, E. *Appl. Surf. Sci.* **1997**, *115*, 386−392.
(29) Valkonen, M. P.; Lindroos, S.; Kanniainen, T.; Leskelä, M.; Tapper, U.; Kauppinen, E. *Appl. Surf. Sci.* **1997**, *120*, 58−64.
(30) Lindroos, S.; Anniainen, T. K.; Leskela, M.; Raukala, E. *Thin Solid Films* **1995**, *263*, 79−84.
(31) Nicolau, Y. F. *Appl. Surf. Sci.* **1984**, *22*, 1061−1074.
(32) Lokhande, C. D.; Pathan, H. M.; Giersig, M.; Tributsch, H. *Appl. Surf. Sci.* **2002**, *187*, 101−107.
(33) Kushiya, K. *Solar Energy* **2004**, *77*, 717−724.
(34) Bhattacharya, R. N.; Ramanathan, K.; Gedvilas, L.; Keyes, B. *J. Phys. Chem. Solids* **2005**, *66*, 1862−1864.
(35) Barbouth, N.; Berthier, Y.; Lincot, D.; Le Thomas, A. *J. Phys. France* **1988**, *49*, 1545−1549.
(36) Yoshida; Yamaguchi, K.; Kazitani, T.; Sugiura, T.; Minoura, H. *J. Electroanal. Chem.* **1999**, *473*, 209−216.
(37) Tomasz, J.; Hrynaszkiewicz, J.; Kozfowski, J.; Cieszynska, E.; Krogulex, T. *J. Electroanal. Chem.* **1994**, *367*, 213−221.
(38) Simon, N.; Gérard, I.; Vigneron, J.; Etcheberry, A. *Thin Solid Films* **2001**, *400*, 134−138.
(39) Beaunier, L.; Cachet, H.; Cortes, R.; Froment, M.; Etcheberry, A. *Thin Solid Films* **2001**, *387*, 108−110.
(40) Ortiz, M. E.; Núñez-Vergara, L. J.; Squella, J. A. *J. Electroanal. Chem.* **2002**, *519*, 46−52.
(41) Donald, S. T.; Chiericato, Jr.; Charles, T. G. A.; Tsuchiya, E. J. *Anal. Chem.* **1982**, *54*, 1720−1725.
(42) McDonagh, C.; MacCraith, B. D.; McEvoy, A. K. *Anal. Chem.* **1998**, *70*, 45−50.
(43) Zhang, X. T.; Liub, Y. C.; Zhang, J. Y.; Lu, Y. M.; Shen, D. Z.; Fan, X. W.; Kong, X. G. *J. Cryst. Growth* **2003**, *254*, 80−84.
(44) Lindroos, S.; Leskelä, M. *Int. J. Inorg. Mater.* **2000**, *2*, 197−201.
(45) Berger, L. I. In *Semiconductor Materials*; CRC Press: CA, 1996; pp 187−198 and 411−447.